Spatial atomic layer deposition on flexible substrates using a modular rotating cylinder reactor

Kashish Sharma and Robert A. Hall
Department of Chemistry and Biochemistry, University of Colorado, Boulder, Colorado 80309

Steven M. George[a)]
Department of Chemistry and Biochemistry, University of Colorado, Boulder, Colorado 80309 and Department of Mechanical Engineering, University of Colorado, Boulder, Colorado 80309

(Received 1 September 2014; accepted 5 November 2014; published 2 December 2014)

Spatial atomic layer deposition (ALD) is a new version of ALD based on the separation of reactant gases in space instead of time. In this paper, the authors present results for spatial ALD on flexible substrates using a modular rotating cylinder reactor. The design for this reactor is based on two concentric cylinders. The outer cylinder remains fixed and contains a series of slits. These slits can accept a wide range of modules that attach from the outside. The modules can easily move between the various slit positions and perform precursor dosing, purging, or pumping. The inner cylinder rotates with the flexible substrate and passes underneath the various spatially separated slits in the outer cylinder. Trimethyl aluminum and ozone were used to grow Al_2O_3 ALD films at 40 °C on metallized polyethylene terephthalate (PET) substrates to characterize this spatial ALD reactor. Spectroscopic ellipsometry measurements revealed a constant Al_2O_3 ALD growth rate of 1.03 Å/cycle with rotation speeds from 40 to 100 RPM with the outer cylinder configured for one Al_2O_3 ALD cycle per rotation. The Al_2O_3 ALD growth rate then decreased at higher rotation rates for reactant residence times < 5 ms. The Al_2O_3 ALD films were also uniform to within <1% across the central portion of metallized PET substrate. Fixed deposition time experiments revealed that Al_2O_3 ALD films could be deposited at 2.08 Å/s at higher rotation speeds of 175 RPM. Even faster deposition rates are possible by adding more modules for additional Al_2O_3 ALD cycles for every one rotation of the inner cylinder.
 [http://dx.doi.org/10.1116/1.4902086]

I. INTRODUCTION

Atomic layer deposition (ALD) is a technique based on sequential, self-limiting surface reactions that produces uniform films with atomic level control of the film thickness.[1] Most ALD processes involve a sequence of reactions where two surface reactions are separated in time. In spatial ALD, the two surface reactions are separated in space rather than time.[2] With this spatial ALD approach, the reactants flow continuously from spatially separated sources and the substrate moves relative to these reactant sources. The deposition rate in spatial ALD is determined by the speed at which the substrate moves past the spatially separated reactant sources.

There have been a variety of approaches to spatial ALD.[2] The original idea of spatial ALD was presented in a patent by Suntola and Antson in 1977.[3] This spatial ALD scheme rotated the substrate between alternating reactant sources and vacuum pumping regions. Subsequently, spatial ALD was reintroduced using a translating gas source head with multiple slits that moved back-and-forth over the substrate.[4,5] The operating conditions have also been evaluated for spatial ALD using a gas source head with multiple slits.[6]

Other designs have improved the definition of the gap between the gas source head and the substrate. One design used a spinning sample with gas bearings to maintain the gap between the gas source head and the substrate.[7–9] Another design used a double gas bearing to "levitate" the translating substrate and define the gap between the gas source head and the substrate.[2,10,11] Other designs employed a rotating drum to move the sample with the gap defined by concentric cylinders.[12,13] Additional designs for roll-to-roll processing have moved the flexible web substrate either through reservoirs of spatially separated reactant sources or under a gas source head with spatially separated reactants.[14,15]

Many parameters need to be varied to optimize the ALD process.[6] These parameters include the reactant exposures, the gap between the gas source head and the substrate, the spatial separation between the reactants, the vacuum pumping rates, and the inert gas flows for purging. Many of the previous spatial ALD reactors have been limited by the restrictive nature of the reactor designs that does not allow for easy adjustments. To circumvent these restrictions, we have designed a new spatial ALD reactor that incorporates elements of the previous designs and allows for great flexibility.

Our new design is inspired by the previous rotating drum design with the gap defined by two concentric cylinders.[12,13] Figure 1 illustrates this design concept for one cycle of Al_2O_3 ALD using trimethylaluminum and ozone as the reactants. The new design incorporates various slit sources on the exterior of the outer cylinder of the reactor. The inner cylinder containing the flexible substrate rotates underneath the various spatially separated slits in the outer cylinder. Each of the modules for reactant dosing, purging, or

[a)]Electronic mail: Steven.George@Colorado.Edu

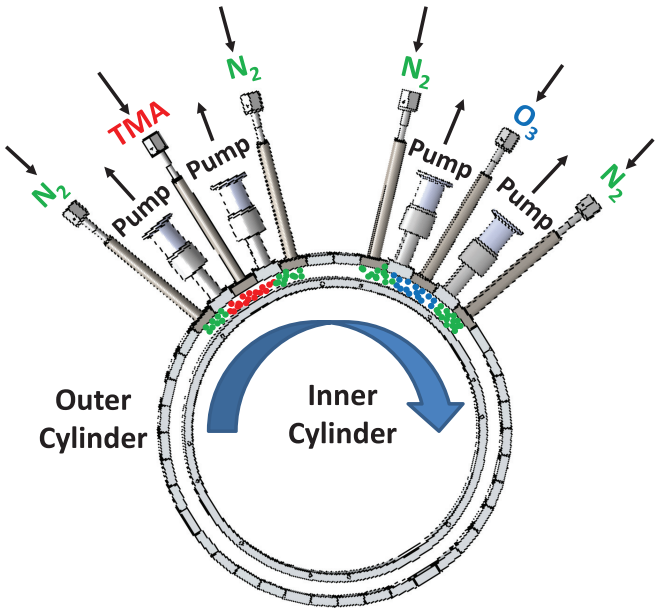

FIG. 1. (Color online) Design concept for modular rotating cylinder reactor showing one cycle of Al_2O_3 ALD using trimethylaluminum and ozone as reactants. Fixed outer cylinder has slits for modules to perform dosing, purging, or pumping. Inner cylinder rotates and passes underneath the slits in outer cylinder.

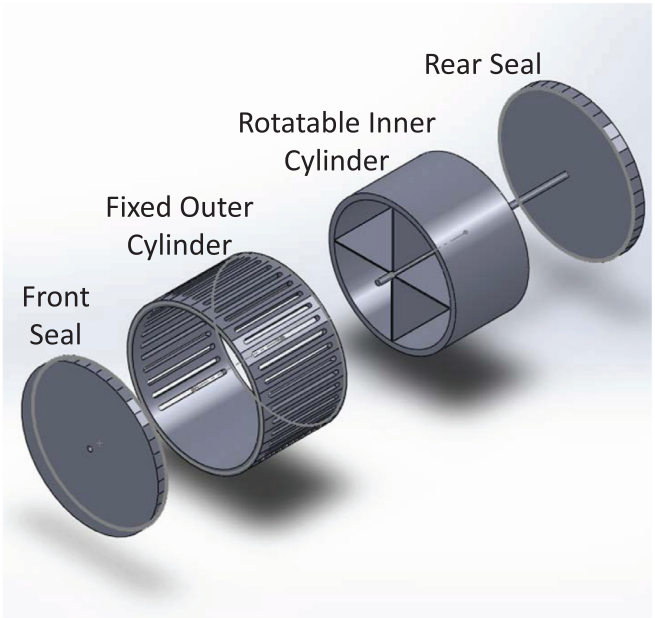

FIG. 2. (Color online) Components of modular rotating cylinder reactor. Modular slits are visible on the fixed outer cylinder.

pumping can be attached to any of the slits on the outer cylinder. The modules can be quickly moved to any of the slit positions to determine the optimal dosing, purging, and pumping positions without having to rebuild the entire reactor.

This modular design was then characterized using Al_2O_3 ALD with trimethylaluminum (TMA) and ozone at 40 °C on metallized polyethylene terephthalate (PET) substrates. Low temperatures are needed for ALD on thermally fragile polymer substrates. Ozone was used instead of H_2O because H_2O purging times are very long at temperatures below 100 °C.[16] In comparison to the difficulties associated with previous designs,[6] Al_2O_3 ALD films were easily grown using the new modular rotating cylinder reactor design. The effect of various reaction parameters on the Al_2O_3 ALD growth rate were studied by varying the ozone process pressures and the speed of the rotating cylinder. The results illustrate that rapid and reliable Al_2O_3 ALD can be obtained on flexible substrates using the modular rotating cylinder reactor for spatial ALD.

II. EXPERIMENT

A. Reactor design

Figure 2 shows the components of the modular rotating cylinder reactor for spatial ALD. There is a fixed outer cylinder and a rotatable inner cylinder. The outer diameters of the inner and outer cylinders are 12.69 and 13.25 in., respectively. The width of the inner cylinder is 7.75 in. The outer cylinder has 31 modular slits around the circumference of the outer cylinder. These 31 slits on the outer cylinder subtend an angle of 270° relative to the cylinder axis. The modular slits are 6.5 in. long and 0.32 in. wide. The distance between the line centers of the modular slits is 1.0 in. The gap between the inner and outer cylinders is 750 μm. The flexible substrate can be fixed to the rotatable inner cylinder. Front and rear circular plates provide for vacuum sealing of the modular rotating cylinder reactor.

A perspective view of the modular rotating cylinder reactor is displayed in Fig. 3. This view illustrates dosing, vacuum, and purge modules in different slit locations on the fixed outer cylinder. Any module can attach at any slit

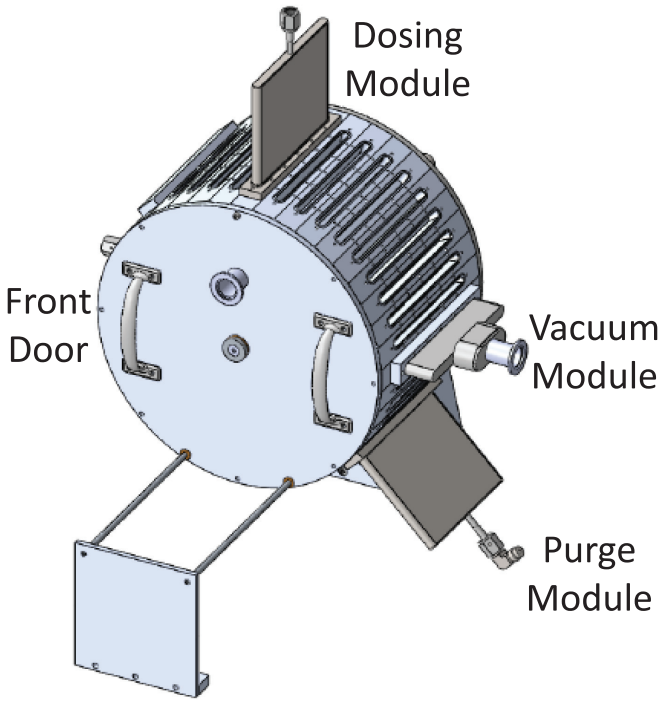

FIG. 3. (Color online) Perspective view of modular rotating cylinder reactor showing dosing, vacuum, and purge modules attached at different slit locations on the fixed outer cylinder.

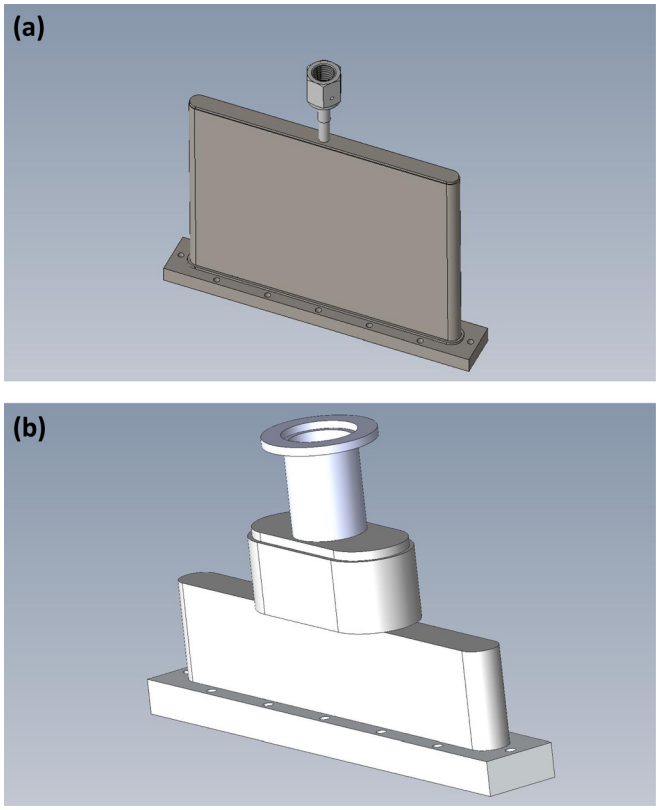

FIG. 4. (Color online) (a) Dosing module and (b) vacuum module that attach to the slits on fixed outer cylinder.

location. This modular design allows the placement of dosing, vacuum, and purging modules anywhere on the outside of the outer cylinder. In addition, the slits can be blanked off to allow greater separation between the dosing, vacuum, and purge modules. This modular design provides great flexibility. Placement of the dosing, vacuum, and purge modules can be changed without requiring machining to rebuild the reactor. Figure 3 also shows a quick connect port on the front door that can be used for a viewport.

More detailed schematics of the dosing and vacuum modules are shown in Fig. 4. The dosing module displayed in Fig. 4(a) is 5.31 in. tall and 6.54 in. wide. The inner spacing between the horizontal plates of the dosing module is 0.34 in., which closely matches the slit width of 0.32 in. This module is connected to the precursor dosing line via a VCR connection that is centered at the top of the dosing module. Computation fluid dynamics simulations revealed that a dosing gas stream traveling through the dosing module will completely fill the width of the dosing module after flowing approximately 2 in. into the dosing module. This behavior ensures that the dosing will be uniform along the length of the 6.5 in. slit.

The vacuum module is illustrated in Fig. 4(b). The vacuum module was designed for maximum pumping speed. The top of the vacuum module connects to a KF 25 quick connect. To achieve maximum pumping speed, the vacuum module has progressively larger inner diameters as the gases move toward the pump. The connection to the slit has an inner spacing of 0.32 in. The linkage to this connection has

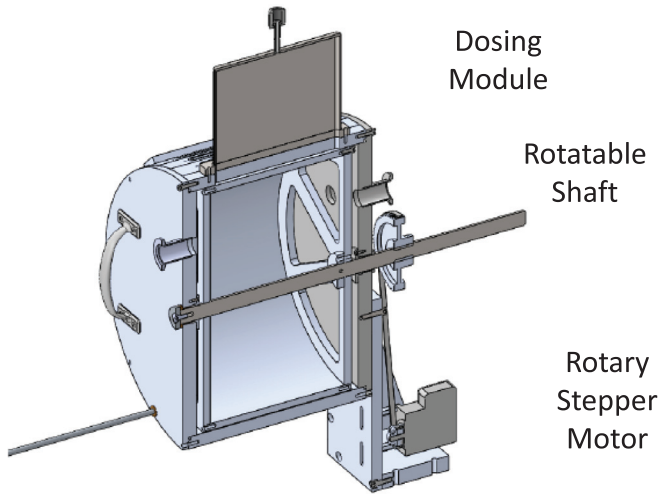

FIG. 5. (Color online) Cross section of the modular rotating cylinder reactor that shows rotatable shaft, rotary stepper motor, and one dosing module positioned on a slit on top of the reactor.

an inner spacing of 0.875 in. before then attaching to the 1.0 in. diameter KF 25 quick connect.

Figure 5 displays the cross section of the modular rotating cylinder reactor. This cut away view shows the rotatable shaft on axis with the inner and outer cylinders. Bearings hold the rotatable shaft concentric with the inner and outer cylinders and also provide a vacuum seal. A dosing module is shown on the top slit of the fixed outer cylinder. The stepper motor is also visible on the back side of the reactor. This stepper motor drives a belt that can rotate the inner cylindrical drum up to 200 RPM. This cut away view also reveals the viewport connection on the front door and two quick

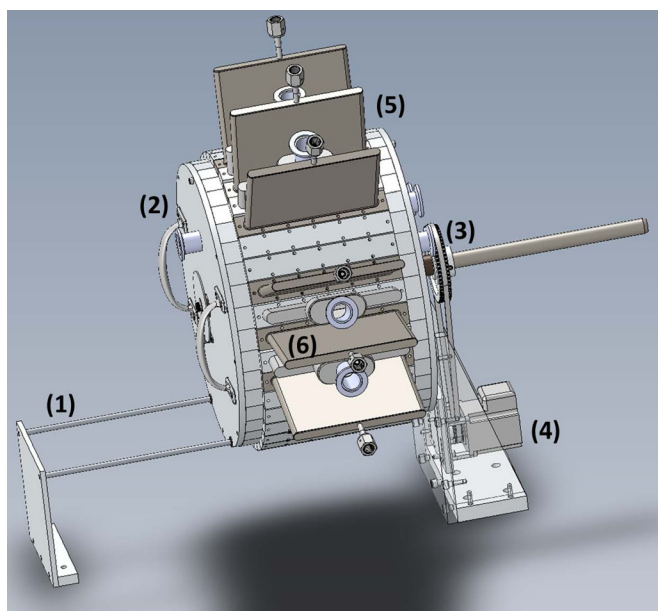

FIG. 6. (Color online) Perspective view of complete reactor showing: (1) railings to move the inner cylinder in and out of outer cylinder; (2) front door; (3) pulley that rotates inner cylinder; (4) stepper rotary motor; (5) first reactant zone that shows dosing module surrounded by vacuum and purging modules; and (6) second reactant zone that shows dosing module surrounded by vacuum and purging modules.

connect ports above the rotatable shaft on the rear seal for vacuum pumping and pressure measurement of the reactor.

A perspective side view of the entire reactor is shown in Fig. 6. This reactor has been outfitted with the dosing, vacuum, and purge modules for two different reactant precursors. For each reactant, the dosing module is contained between two vacuum modules. Purge modules are on each side of the vacuum modules to prevent the mixing of reactants. Railings that allow the inner cylinder to slide out of the fixed outer cylinder are positioned on the left-hand side of the reactor. The rotatable shaft and stepper motor are on the right-hand side of the reactor.

With the configuration shown in Fig. 6 with two reactant precursors, one RPM yields one complete ALD cycle. Using a purge/pump/dose/pump/purge module sequence with no blank modules, three complete ALD cycles can be achieved in one revolution with the 31 modular slits. The bottom of the fixed outer cylinder has been left blank at this time. In the future, this empty section could be used to bring a web material into and out of the reactor for roll-to-roll processing. This introduction of roll-to-roll capability would require differential pumping of the web material entering and leaving the reactor.

A photograph of the front of the modular rotating cylinder reactor is displayed in Fig. 7. The purge/pump/dose/pump/purge module sequence for TMA is on the left-hand side of the reactor. The purge/pump/dose/pump/purge module sequence for O_3 is on the right-hand side of the reactor. This configuration was used for the Al_2O_3 ALD growth characterization presented in Sec. II B. The picture also shows the railing for moving the rotatable inner cylinder in and out of the reactor defined by the fixed outer cylinder. The quick connection port intended for a viewport has been blanked off.

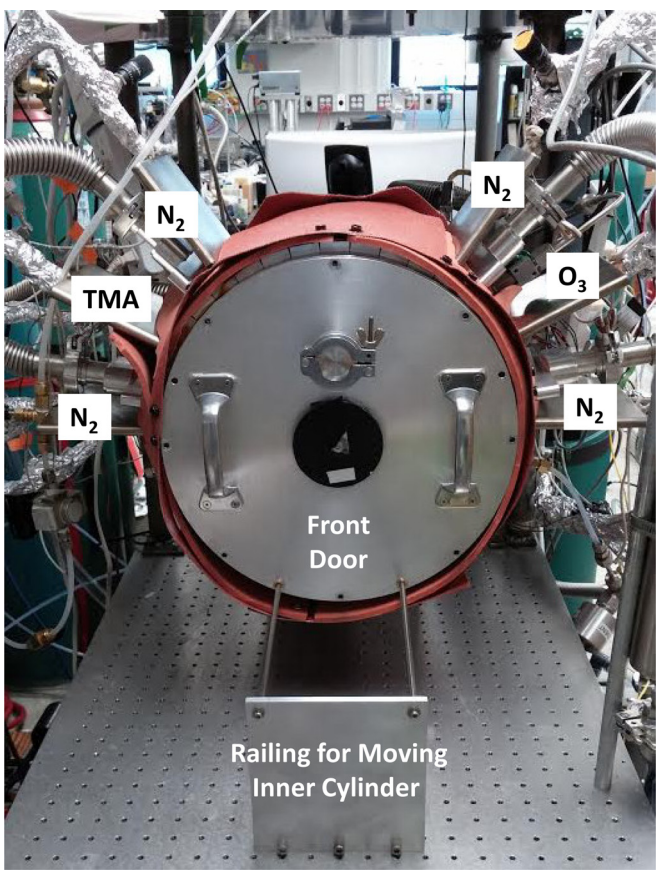

FIG. 7. (Color online) Photograph of front of modular rotating cylinder reactor with TMA reactant zone on the left-hand side and O_3 reactant zone on the right-hand side. Picture also shows front door of reactor and railing to move inner cylinder into and out of the fixed outer cylinder.

B. Growth and characterization of Al_2O_3 ALD films

To characterize the new modular rotating cylinder reactor, Al_2O_3 ALD films were deposited on metallized PET substrates using TMA and ozone as the reactants. Al_2O_3 ALD using TMA and ozone has been characterized previously by a number of studies.[17–23] The PET substrates had a thickness of 130 μm. The metal coating on the PET substrates was sputtered titanium. The temperature of the fixed outer cylinder was 60 °C. The temperature of the rotating inner cylindrical drum was 40 °C. This temperature was measured immediately after opening the front door of the reactor after the fixed outer cylinder had been at 60 °C for several hours. The PET samples were attached to the inner cylinder using Kapton tape.

The samples were allowed to thermally equilibrate on the inner cylindrical drum for 30 min. Ultrahigh purity nitrogen was flowed continuously for 30 min. to assist the heat transfer from the outer cylinder to the inner cylinder. The whole reactor was pumped down using a dual stage rotary vane mechanical pump to the base pressure of ~40 mTorr. This base pressure was obtained without any gas load into the reactor.

TMA (AKZO Nobel HPMO) was used as a reactant gas. N_2 gas was bubbled through the TMA canister using a N_2 gas flow. The output line from the TMA canister was connected to the TMA dosing module using a pneumatic valve and a needle valve to control the TMA/N_2 gas flow. Purging was accomplished using a N_2 flow of 200 sccm in each purging module. A separate dual stage rotary vane mechanical pump was utilized to pump unreacted TMA reactants, reaction products, and the N_2 purge.

O_3 was produced using an O3ONIA ozone generator where oxygen (Airgas) was used as a source gas. The product O_3 was at a concentration of ~10% in the O_2 gas flow. The gas flow from the O_3 generator to the O_3 dosing module was controlled using a pneumatic valve and a needle valve. The process pressure in the O_3 dosing module was increased by enlarging the flow into the O_3 dosing module. This process pressure includes both O_3 and O_2. A separate dual stage rotary vane mechanical pump was utilized to pump the O_3 dosing module. An ozone destruct unit (Ozone Solutions Inc.) was utilized to react O_3 to O_2 before the reaction products reached the mechanical pump.

Three dual stage rotary vane pumps were used to pump the TMA reaction channel, the O_3/O_2 reaction channel and the reactor chamber. Process pressures ranging between 10 and 19 Torr were measured in the O_3/O_2 dosing module. A pressure of 15 Torr was measured in the TMA dosing module. During Al_2O_3 ALD, the pressure in the reactor chamber was ~11 Torr.

The thicknesses of the Al_2O_3 ALD films on the metallized PET substrates were determined with spectroscopic

ellipsometry. A visible ellipsometer (J A Woollam Co., Inc., M2000U) was used to perform these measurements. The film thickness and the dispersion relation of the optical constants over the photon energy range can be deduced from the ellipsometric data. A standard Cauchy model was used to fit the dispersion of the refractive index using the A_n, B_n, and C_n Cauchy fit parameters.[24]

X-ray photoemission spectroscopy (XPS) analysis was performed using a PHI 5600 x-ray photoelectron spectrometer using a monochromatic Al Kα source. The XPS depth-profiling to remove the surface carbon was conducted using argon sputtering. The XPS data were collected using Auger Scan (RBD Enterprises, Inc., Bend, OR). The XPS data were analyzed in CASA XPS (Casa Software Ltd., UK).

III. RESULTS AND DISCUSSION

Figure 8 shows the Al_2O_3 ALD film thickness versus number of Al_2O_3 ALD cycles at 40 °C, an O_3/O_2 process pressure of 18 Torr, and 100 RPM. The Al_2O_3 ALD film growth is very linear with number of Al_2O_3 ALD cycles. The slope of the Al_2O_3 ALD film thickness versus number of Al_2O_3 ALD cycles yields a growth per cycle (GPC) of 1.02 ± 0.01 Å/cycle at 40 °C. This growth rate is slightly less than the growth rate of 1.1–1.2 Å/cycle commonly measured for Al_2O_3 ALD using TMA and H_2O at temperatures between 33 and 177 °C.[16,25–27]

The Al_2O_3 ALD growth rate is dependent on the O_3/O_2 process pressure. Figure 9 displays the Al_2O_3 ALD growth rate versus O_3/O_2 process pressure at 40 °C and 100 RPM. The process pressure was adjusted by increasing the O_3/O_2 gas flow from the ozone generator. The Al_2O_3 ALD growth rate increased with process pressure and reached an Al_2O_3 ALD growth rate of 1.03 Å/cycle at $\geq$18 Torr.

This nearly linear dependence of Al_2O_3 ALD growth rate on O_3/O_2 process pressure suggests that the surface reactions have not saturated at lower process pressures $<$ 18 Torr at 40 °C and 100 RPM. The maximum Al_2O_3 ALD growth rate of 1.03 Å/cycle was observed at process pressures of 18–19 Torr at a rotation rate of 100 RPM. Process pressures $>$ 19 Torr were observed to lead to Al_2O_3 chemical vapor deposition (CVD) in the reactor. The signature of Al_2O_3 CVD is a powdery white film on the edges of the inner rotating cylinder.

Figure 10 shows the dependence of the Al_2O_3 ALD growth rate on the rotation rate at 40 °C and an O_3/O_2 process pressure of 18 Torr. The Al_2O_3 ALD growth rate was determined by dividing the Al_2O_3 ALD film thickness by the total number of Al_2O_3 ALD cycles completed after a deposition time of 5 min. The Al_2O_3 ALD growth rate increases with decreasing rotation rate. The Al_2O_3 ALD growth rate has a maximum growth rate at 1.03 Å/cycle at $\leq$100 RPM. The growth rate of 1.03 Å/cycle at 40 °C and $\leq$100 RPM can be compared with Al_2O_3 ALD growth rates measured by other studies using TMA and O_3 at higher temperatures.

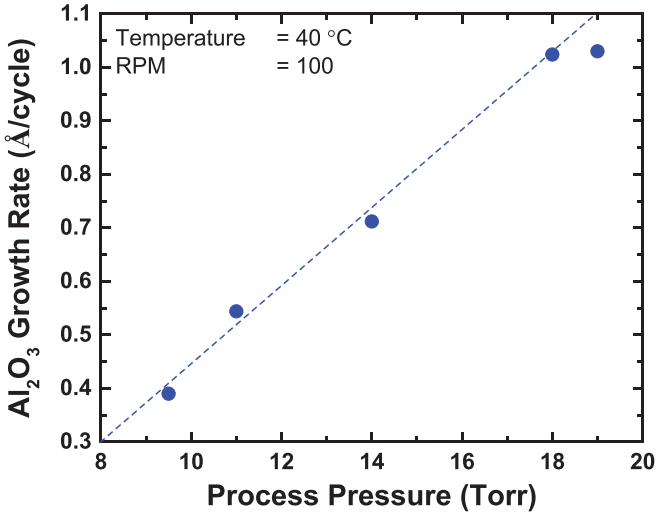

FIG. 9. (Color online) Al_2O_3 growth rate vs O_3/O_2 process pressure at 40 °C, 100 RPM, and a TMA pressure of 15 Torr. The Al_2O_3 growth rate increases linearly with the O_3/O_2 process pressure.

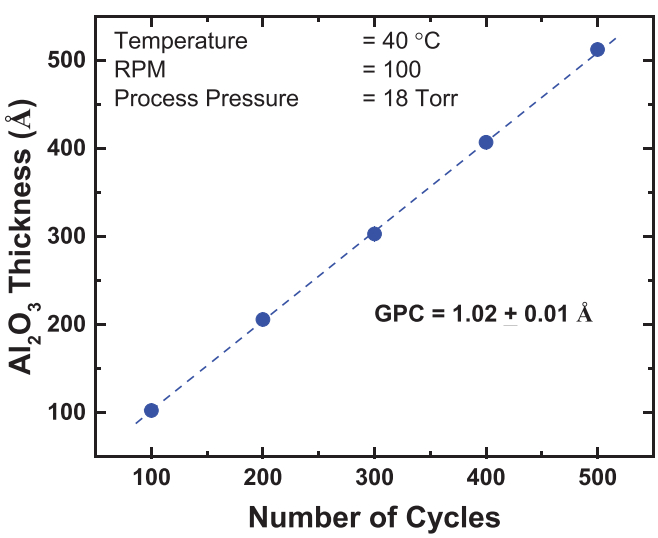

FIG. 8. (Color online) Al_2O_3 thickness vs number of Al_2O_3 ALD cycles at 40 °C, 100 RPM, an O_3/O_2 process pressure of 18 Torr, and a TMA pressure of 15 Torr. The Al_2O_3 ALD GPC is 1.02 ± 0.01 Å/cycle.

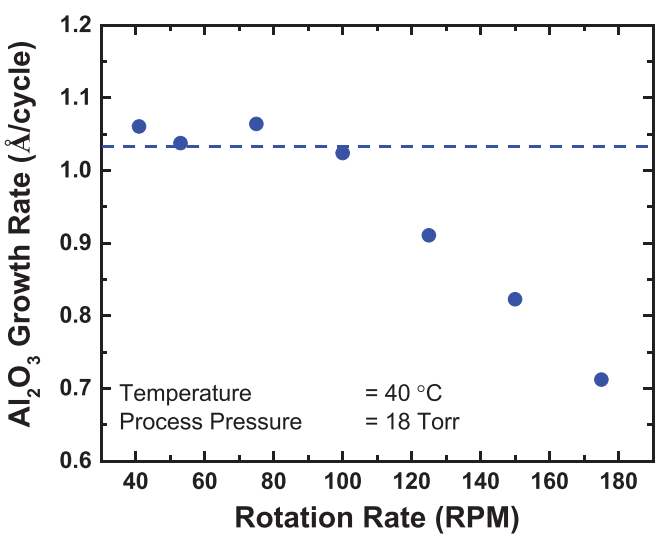

FIG. 10. (Color online) Al_2O_3 growth rate vs rotation rate. Growth rate is constant at 1.03 Å/cycle up to 100 RPM. Additional increase in rotation rate leads to a progressive decrease in the growth rate.

The growth rate of 1.03 Å/cycle at 40 °C and ≤100 RPM is somewhat less that the growth rate of 1.2 Å/cycle measured at 70 °C.[23] The growth rate of 1.03 Å/cycle is also less than the growth rate of 1.3 and 1.1 Å/cycle obtained earlier at higher temperatures of 150 and 277 °C, respectively.[17,18] In contrast, the growth rate of 1.03 Å/cycle is greater than the growth rates of 0.6, 0.85, and 0.75 Å/cycle, measured at much higher temperatures of 350, 380, and 450 °C, respectively.[19,28,29] The decrease of the Al_2O_3 ALD growth rate at progressively higher temperatures from 150 to 300 °C has been observed by previous x-ray reflectivity measurements.[17] However, other studies have observed a constant growth rate of 0.9 Å/cycle at 150–250 °C.[23]

The Al_2O_3 ALD growth rates using the modular rotating cylinder reactor with TMA and ozone are also similar to the Al_2O_3 ALD growth rates observed in other spatial ALD reactors with TMA and H_2O as the reactants. Previous results in a rotating drum reactor obtained Al_2O_3 ALD growth rates of 1.0–1.2 Å/cycle on flexible substrates using TMA and water as the reactants at 100–150 °C.[12,13] Previous results using a spinning sample with gas bearings reactor reported Al_2O_3 ALD growth rates of 1.2 Å/cycle on silicon wafers using TMA and water as the reactants at 200 °C.[9]

The Al_2O_3 ALD growth rate in Fig. 10 is constant with rotation rate up to ~100 RPM. Subsequently, the Al_2O_3 ALD growth rate decreases progressively at higher rotation rates. This decrease at higher rotation rates suggests that the reactant exposures are not sufficient for the TMA and/or O_3 surface reactions to reach completion at the higher rotation rates. The TMA and/or O_3 reactant residence times are likely not sufficient for the saturation of the surface reactions at >100 RPM.[26,27,30]

For our modular rotating cylinder reactor, the outer diameter of the inner cylinder is 12.69 in. and the circumference of the inner cylinder is 39.9 in. or 1.0 m. At a rotation rate of 100 RPM, the flexible substrate moves at a velocity of 66.5 in./s or 1.7 m/s relative to the slits on the outer cylinder. Assuming a reaction zone width equal to the slit width of 0.32 in., the reactant residence time is 4.8 ms. Figure 10 shows that the Al_2O_3 ALD growth rates have the maximum Al_2O_3 growth rate of 1.03 Å/cycle for residence times ≥ 5 ms obtained for rotation rates ≤ 100 RPM. For rotation rates > 100 RPM, the Al_2O_3 ALD growth rate decreases at 125, 150, and 175 RPM when the residences times are 4.0, 3.3, and 2.7 ms, respectively.

The uniformity of the Al_2O_3 ALD film thickness was also evaluated using spectroscopic ellipsometry measurements after deposition on metallized PET substrates that were 40 in. long and 7.5 in. wide. Figure 11 shows the Al_2O_3 ALD film thickness versus substrate position across the width of the flexible polymer substrate. The thickness is very uniform at ~650 Å after 700 Al_2O_3 ALD cycles. This thickness is consistent with an Al_2O_3 ALD growth rate of 0.93 Å/cycle at a process pressure of 17 Torr.

The uniformity is excellent with thickness variations of only <1% across the middle 4.5 in. section of the substrate. The Al_2O_3 thickness is slightly higher at the edge of the slits that have a length of 6.5 in. This slightly larger growth rate could be attributed to some Al_2O_3 CVD. This Al_2O_3 CVD may be caused by some mixing of the TMA and O_3 precursors resulting from lower pumping and purging at the ends of the slit modules. The larger Al_2O_3 thicknesses at the ends of the slit modules are only <3% larger than the very uniform thickness of ~650 Å in the middle section of the substrate.

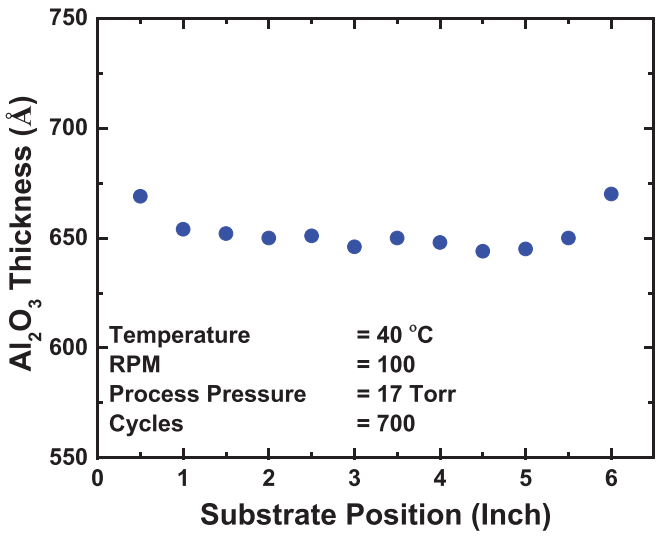

FIG. 11. (Color online) Al_2O_3 thickness vs substrate position across the width of metallized PET substrate. Al_2O_3 thickness was grown using 700 cycles at 100 RPM and a process pressure of 17 Torr.

Spectroscopic ellipsometry analysis measured a refractive index of $n = 1.50 \pm 0.02$ for all the Al_2O_3 ALD films on the metallized PET substrates. This refractive index is consistent with the refractive index of $n = 1.51$ measured earlier for Al_2O_3 ALD films grown at 33 °C using TMA and H_2O.[16] XPS analysis also measured a low carbon content of ~2 at. % in Al_2O_3 ALD films deposited at 40 °C, 100 RPM, an O_3/O_2 process pressure of 18 Torr, and a TMA pressure of 15 Torr. This carbon content was measured after sputtering through the adventitious carbon on the surface of the Al_2O_3 film.

The measurements used to obtain the Al_2O_3 ALD growth rate versus rotation rate in Fig. 10 can also be employed to determine the Al_2O_3 film thickness versus rotation rate after a deposition time of 5 min. Figure 12 shows that larger Al_2O_3 ALD film thicknesses are observed at higher rotations rates after a fixed deposition time of 5 min. The dashed line shows the expected Al_2O_3 thicknesses versus rotation rate for an Al_2O_3 ALD growth rate of 1.03 Å/cycle. The dependence between Al_2O_3 ALD film thickness and rotation rate is nearly linear up to ~100 RPM in agreement with the results in Fig. 10.

Figure 12 can be used to determine the speed in depositing the Al_2O_3 ALD films. Based on the deposition of an Al_2O_3 ALD film thickness of 623 Å in 5 min at 175 RPM, the Al_2O_3 ALD growth rate is 2.08 Å/s. Although Fig. 10 shows the Al_2O_3 ALD growth rate per cycle is not the highest at 175 RPM, the highest Al_2O_3 ALD growth rate per time is achieved at 175 RPM. This result was obtained with the outer cylinder configured for one Al_2O_3 ALD cycle per rotation.

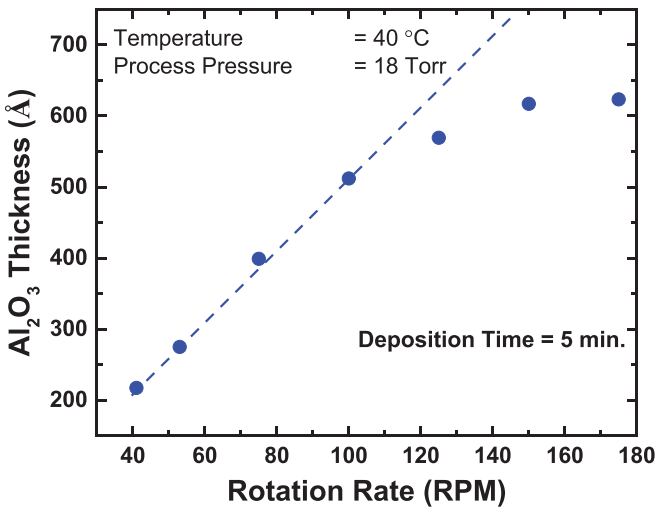

FIG. 12. (Color online) Al_2O_3 thickness vs rotation rate for a deposition time of 5 min. Al_2O_3 thickness is consistent with Al_2O_3 ALD growth rate of 1.03 Å/cycle for rotation rates up to 100 RPM.

Even faster deposition rates are possible by adding more modules for additional Al_2O_3 ALD cycles for every one rotation of the inner cylinder. The current modular rotating cylinder design could accommodate up to three Al_2O_3 ALD cycles per rotation. Consequently, the Al_2O_3 ALD growth rate at 40 °C could be extended to 6.24 Å/s at 175 RPM if there is sufficient spatial separation during the three Al_2O_3 ALD cycles to prevent Al_2O_3 CVD.

One major difference between the spatial ALD results for Al_2O_3 ALD obtained in this study with TMA and O_3 and previous studies using TMA and H_2O is the dependence of the Al_2O_3 ALD growth rate on the speed of the substrate. In the rotating drum reactor, the speed of the substrate is measured by the RPM rate.[12] In the spinning sample with gas bearings reactor, the speed of the substrate is measured by the inverse of the rotation frequency and the radius of the sample position.[8] In both cases, the speed of the substrate can be converted to a residence time for the reactants on the surface and the time period between adjacent reactant exposures.[8,12]

For the reactor configuration for one cycle of Al_2O_3 ALD shown in Fig. 7, the TMA and O_3 reaction zones are separated by ~14 in. and the separation time between the TMA and O_3 reactant exposures is ~210 ms at 100 RPM. In comparison, the O_3 and TMA reaction zones are separated by ~26 in. and the separation time between the O_3 and TMA reactant exposures is ~390 ms at 100 RPM. By moving the reactant modules closer or further apart, the separation times can be varied between 60 and 540 ms at 100 RPM.

For Al_2O_3 ALD using TMA and H_2O as the reactants in spatial ALD reactors, the Al_2O_3 growth rates can increase dramatically at shorter separation times and lower substrate temperatures ≤ 100 °C.[8,12] This increase is attributed to H_2O that is not purged from the surface in the time between reactant exposures.[8,12] This extra H_2O can react with TMA and leads to increased Al_2O_3 growth rates resulting from Al_2O_3 CVD.[8,12] In contrast, the Al_2O_3 ALD growth rate versus rotation rate in Fig. 10 using TMA and ozone at 40 °C does not display any evidence for Al_2O_3 CVD at higher rotation rates and short time periods between TMA and ozone exposures.

This absence of Al_2O_3 CVD is consistent with the much higher pumping rate of O_3 compared with H_2O. H_2O is very sticky and difficult to pump especially at low temperatures < 100 °C.[16] Ozone is more easily purged from the surface than H_2O and is not pulled into the TMA reaction zone by the substrate. Consequently, ozone is a more desirable oxidant than H_2O to avoid Al_2O_3 CVD effects at lower temperature and higher substrate speeds.

Our future research will focus on ALD on porous electrodes on flexible metal foil. These porous electrodes are utilized to fabricate Li ion batteries. Recent work has demonstrated that Al_2O_3 ALD coatings on these porous electrodes can dramatically improve the capacity stability of Li ion batteries.[31–33] These porous electrodes will offer an additional challenge for spatial ALD because of the limited gas conductance for porous substrates.

To confront this challenge, we will utilize a "push–pull" design where the pressure of the precursor dose will "push" the precursors into the porous electrode. The reaction products and unreacted precursors will then be "pulled" from the porous electrode by vacuum pumping. A "push" pressure in viscous flow at ~1 Torr and a "pull" pressure in molecular flow at ~100 mTorr may be a good combination of pressures for ALD in these porous substrates.

IV. CONCLUSIONS

A new spatial ALD reactor was developed based on a modular rotating cylinder design. There are two concentric cylinders in this design. The outer cylinder remains fixed and contains a series of slits. The slits can accept a wide range of modules that attach from the outside and accommodate precursor dosing, purging, and pumping modules. The inner cylinder rotates and passes underneath the various spatially separated slits in the outer cylinder. The modules can be positioned on any of the slits to optimize the ALD processing without having to remachine the reactor.

This new spatial ALD reactor was used to characterize Al_2O_3 ALD using TMA and ozone as the reactants. Al_2O_3 ALD films were grown at 40 °C on metallized PET substrates using modules on the outer cylinder for one Al_2O_3 ALD cycle per rotation. The Al_2O_3 ALD growth rate was constant at 1.03 Å/cycle between rotation rates of 40 and 100 RPM. The Al_2O_3 ALD growth rate then decreased at higher rotation rates >100 RPM. This decrease was attributed to reactant residence times <5 ms that are insufficient for the surface reactions to reach completion. The Al_2O_3 ALD films were also uniform to within <1% across the center portion of the metallized PET substrates.

Fixed deposition time experiments revealed that the Al_2O_3 ALD growth rate versus time reached the maximum value of 2.08 Å/s at the highest rotation rate of 175 RPM. The current modular rotating cylinder design would accommodate up to three Al_2O_3 ALD cycles per rotation. Consequently, the Al_2O_3 ALD growth rate at 40 °C could be extended to 6.24 Å/s at 175 RPM if there is sufficient spatial

separation during the three Al_2O_3 ALD cycles to prevent Al_2O_3 CVD. These high deposition rates would allow very rapid ALD processing of flexible substrates.

ACKNOWLEDGMENTS

This research was supported by the National Science Foundation through SNM: Roll-to-Roll Atomic/Molecular Layer Deposition (CBET 1246854). Additional support was contributed by the Department of Energy through funding from the National Renewable Energy Laboratory (NREL). Some of the components used to construct the spatial ALD reactor were provided by the Defense Advanced Research Project Agency (DARPA). The authors would like to thank Jim Kastengren and Don David in the CIRES/Chemistry Integrated Instrument Development Facility for their invaluable help with the design and construction of this reactor. The authors would also like to thank Tommi Kaariainen and David Cameron for furnishing the metallized PET substrates.

[1]S. M. George, Chem. Rev. **110**, 111 (2010).
[2]P. Poodt, D. C. Cameron, E. Dickey, S. M. George, V. Kuznetsov, G. N. Parsons, F. Roozeboom, G. Sundaram, and A. Vermeer, J. Vac. Sci. Technol., A **30**, 010802 (2012).
[3]T. Suntola and J. Antson, U.S. patent 4,058,430 (15 November 1977).
[4]D. H. Levy, D. Freeman, S. F. Nelson, P. J. Cowdery-Corvan, and L. M. Irving, Appl. Phys. Lett. **92**, 192101 (2008).
[5]D. H. Levy, S. F. Nelson, and D. Freeman, J. Display Technol. **5**, 484 (2009).
[6]P. R. Fitzpatrick, Z. M. Gibbs, and S. M. George, J. Vac. Sci. Technol., A **30**, 01A136 (2012).
[7]A. Illiberi, F. Roozeboom, and P. Poodt, ACS Appl. Mater. Interfaces **4**, 268 (2012).
[8]P. Poodt, A. Illiberi, and F. Roozeboom, Thin Solid Films **532**, 22 (2013).
[9]P. Poodt, A. Lankhorst, F. Roozeboom, K. Spee, D. Maas, and A. Vermeer, Adv. Mater. **22**, 3564 (2010).
[10]V. I. Kuznetsov, E. H. A. Granneman, P. Vermont, and K. Vanormelingen, ECS Trans. **33**, 441 (2010).
[11]F. Werner, W. Stals, R. Goertzen, B. Veith, R. Brendel, and J. Schmidt, Energy Procedia **8**, 301 (2011).
[12]P. S. Maydannik, T. O. Kaariainen, and D. C. Cameron, Chem. Eng. J. **171**, 345 (2011).
[13]P. S. Maydannik, T. O. Kaariainen, and D. C. Cameron, J. Vac. Sci. Technol., A **30**, 01A122 (2012).
[14]E. Dickey and W. A. Barrow, J. Vac. Sci. Technol., A **30**, 021502 (2012).
[15]A. S. Yersak, Y. C. Lee, J. A. Spencer, and M. D. Groner, J. Vac. Sci. Technol., A **32**, 01A130 (2014).
[16]M. D. Groner, F. H. Fabreguette, J. W. Elam, and S. M. George, Chem. Mater. **16**, 639 (2004).
[17]S. D. Elliott, G. Scarel, C. Wiemer, M. Fanciulli, and G. Pavia, Chem. Mater. **18**, 3764 (2006).
[18]D. N. Goldstein, J. A. McCormick, and S. M. George, J. Phys. Chem. C **112**, 19530 (2008).
[19]S. C. Ha, E. Choi, S. H. Kim, and J. S. Roh, Thin Solid Films **476**, 252 (2005).
[20]J. B. Kim, D. R. Kwon, K. Chakrabarti, C. Lee, K. Y. Oh, and J. H. Lee, J. Appl. Phys. **92**, 6739 (2002).
[21]J. Kwon, M. Dai, M. D. Halls, and Y. J. Chabal, Chem. Mater. **20**, 3248 (2008).
[22]M. Rose, J. Niinistoe, I. Endler, J. W. Bartha, P. Kuecher, and M. Ritala, ACS Appl. Mater. Interfaces **2**, 347 (2010).
[23]M. B. M. Mousa, C. J. Oldham, and G. N. Parsons, Langmuir **30**, 3741 (2014).
[24]E. Langereis, S. B. S. Heil, H. C. M. Knoops, W. Keuning, M. C. M. van de Sanden, and W. M. M. Kessels, J. Phys. D: Appl. Phys. **42**, 073001 (2009).
[25]J. W. Elam, M. D. Groner, and S. M. George, Rev. Sci. Instrum. **73**, 2981 (2002).
[26]A. W. Ott, J. W. Klaus, J. M. Johnson, and S. M. George, Thin Solid Films **292**, 135 (1997).
[27]R. L. Puurunen, J. Appl. Phys. **97**, 121301 (2005).
[28]J. Kim, K. Chakrabarti, J. Lee, K. Y. Oh, and C. Lee, Mater. Chem. Phys. **78**, 733 (2003).
[29]T. P. Lee, C. Jang, B. Haselden, M. Dong, S. Park, L. Bartholomew, H. Chatham, and Y. Senzaki, J. Vac. Sci. Technol., B **22**, 2295 (2004).
[30]P. Poodt, J. van Lieshout, A. Illiberi, R. Knaapen, F. Roozeboom, and A. van Asten, J. Vac. Sci. Technol., A **31**, 01A108 (2013).
[31]Y. S. Jung, A. S. Cavanagh, A. C. Dillon, M. D. Groner, S. M. George, and S.-H. Lee, J. Electrochem. Soc. **157**, A75 (2010).
[32]Y. S. Jung, A. S. Cavanagh, L. A. Riley, S.-H. Kang, A. C. Dillon, M. D. Groner, S. M. George, and S.-H. Lee, Adv. Mater. **22**, 2172 (2010).
[33]I. D. Scott, Y. S. Jung, A. S. Cavanagh, Y. An, A. C. Dillon, S. M. George, and S.-H. Lee, Nano Lett. **11**, 414 (2011).